Interaction of Benzoate Pyrimidine Analogues with Class 1A Dihydroorotate Dehydrogenase from *Lactococcus lactis*[†,‡]

Abigail E. Wolfe,[§] Majbritt Thymark,[||,⊥] Samuel G. Gattis,[§] Rebecca L. Fagan,[§] Yu-chen Hu,[§] Eva Johansson,[||,#] Susan Arent,[||] Sine Larsen,[||,#] and Bruce A. Palfey*[,§]

Department of Biological Chemistry, University of Michigan Medical School, 1150 West Medical Center Drive, Ann Arbor, Michigan 48109-0606, Department of Chemistry, Universitetsparken 5, 2100 Copenhagen, Denmark, Department of Clinical Microbiology, Copenhagen University Hospital, Denmark, and European Synchrotron Radiation Facility (ESRF), B.P. 220, 38043 Grenoble, France

Received January 24, 2007; Revised Manuscript Received March 15, 2007

ABSTRACT: Dihydroorotate dehydrogenases (DHODs) catalyze the oxidation of dihydroorotate to orotate in the only redox reaction in pyrimidine biosynthesis. The pyrimidine binding sites are very similar in all structurally characterized DHODs, suggesting that the prospects for identifying a class-specific inhibitor directed against this site are poor. Nonetheless, two compounds that bind specifically to the Class 1A DHOD from *Lactococcus lactis*, 3,4-dihydroxybenzoate (3,4-diOHB) and 3,5-dihydroxybenzoate (3,5-diOHB), have been identified [Palfey et al. (2001) *J. Med. Chem. 44*, 2861−2864]. The mechanism of inhibitor binding to the Class 1A DHOD from *L. lactis* has now been studied in detail and is reported here. Titrations showed that 3,4-diOHB binds more tightly at higher pH, whereas the opposite is true for 3,5-diOHB. Isothermal titration calorimetry and absorbance spectroscopy showed that 3,4-diOHB ionizes to the phenolate upon binding to the enzyme, but 3,5-diOHB does not. The charge-transfer band that forms in the 3,4-diOHB complex allowed the kinetics of binding to be observed in stopped-flow experiments. Binding was slow enough to observe from pH 6 to pH 8 and was (minimally) a two-step process consisting of the rapid formation of a complex that isomerized to the final charge-transfer complex. Orotate and 3,5-diOHB bind too quickly to follow directly, but their dissociation kinetics were studied by competition and described adequately with a single step. Crystal structures of both inhibitor complexes were determined, showing that 3,5-diOHB binds in the same orientation as orotate. In contrast, 3,4-diOHB binds in a twisted orientation, enabling one of its phenolic oxygens to form a very strong hydrogen bond to an asparagine, thus stabilizing the phenolate and causing charge-transfer interactions with the π-system of the flavin, resulting in a green color.

Dihydroorotate dehydrogenase (DHOD[1]), a flavoprotein, catalyzes the only redox step in *de novo* pyrimidine biosynthesis. The enzyme-bound FMN is reduced in the oxidation of dihydroorotate (DHO) to form orotate and is then reoxidized by different electron acceptors that depend on the source of the enzyme. A comparison of amino acid sequences allows DHODs to be separated into two major classes (*1*), and Class 1 DHODs have been further categorized into two groups (1A and 1B). Class 1 enzymes are cytosolic. Class 1A DHODs are homodimers, and fumarate is assumed to be the physiological electron-accepting substrate (*2*). Class 1B DHODs are heterotetramers and use NAD^+ as the electron acceptor (*3*). The Class 2 DHODs are membrane-bound monomers that utilize respiratory quinones to accept electrons (*4*). Class 1 DHODs are mainly found in Gram-positive bacteria, whereas the Class 2 enzymes are found in Gram-negative bacteria and most eukaryotes. An interesting exception is the occurrence of Class 1A DHODs in some disease-causing protozoans, making them possible drug targets in the treatment of Leishmaniasis, Chagas' disease, and African sleeping sickness.

Class 1A DHODs contain only a single active site, which alternately binds DHO and fumarate in a ping−pong catalytic cycle (*1*), whereas the Class 1B and Class 2 enzymes have one substrate binding site for DHO and a second for NAD^+ or ubiquinone, respectively (*3*, *4*). The orotate/DHO binding sites are nearly identical in the different classes of DHODs. Crystal structures with orotate bound have been solved for each class of enzyme (*5*−*9*). Not only is the geometry very similar but also key residues in the active sites are highly conserved. Each site contains an FMN and an orotate, which is stacked parallel to the isoalloxazine ring. A highly conserved flexible loop covers the active site. A residue on

[†] This work was supported by NIH Grant GM61087 and the Danish National Research Foundation. R.L.F. was supported by NIGMS training grant GM07767.

[‡] Atomic coordinates and structure factors have been deposited with the Protein Data Bank under accession codes 2BSL and 2BX7.

* To whom correspondence should be addressed. Phone: (734) 615-2452. Fax: (734) 764-3509. E-mail: brupalf@umich.edu.

[§] University of Michigan Medical School.

[||] Universitetsparken 5.

[⊥] Copenhagen University Hospital.

[#] European Synchrotron Radiation Facility (ESRF).

[1] Abbreviations: 3,4-diOHB, 3,4-dihydroxybenzoate; 3,5-diOHB, 3,5-dihydroxybenzoate; DHO, dihydroorotate; DHOD, dihydroorotate dehydrogenase; DHOD A, Class 1A DHOD; ITC, isothermal titration calorimetry; KP_i, potassium phosphate buffer; NCS, non-crystallographic symmetry; AMPSO, *N*-(1,1-dimethyl-2-hydroxyethyl)-3-amino-2-hydroxypropanesulfonic acid; CHES, 2-(cyclohexylamino)-ethanesulfonic acid; MOPS, 3-(*N*-morpholino)-propanesulfonic acid.

10.1021/bi7001554 CCC: $37.00
Published on Web 04/20/2007

the loop, Cys in Class 1 DHODs and Ser in Class 2 DHODs, is in close contact with C5 of bound orotate and acts as a base during DHO oxidation. After DHO oxidation, the loop opens in the Class 1A enzymes, releasing orotate (*5*). Kinetic studies have shown that orotate release is too slow to be catalytically relevant in the Class 2 enzymes (*10*). In each of the three classes of DHODs, conserved residues form hydrogen bonds with orotate and presumably also with DHO. A totally conserved Lys residue forms hydrogen bonds with N5 of FMN and the carboxylate group of orotate. Three Asn residues form hydrogen bonds with the nitrogen atoms and carbonyl oxygens of the pyrimidine ring, resulting in a cyclic hydrogen-bonded system for two of these. Finally, either a Ser (Class 1) or a Thr (Class 2) forms a hydrogen bond with a carbonyl oxygen, maximizing the hydrogen-bonding interactions with the bound pyrimidine moiety. The highly conserved array of binding residues makes the pyrimidine binding sites in the different classes of DHODs appear almost indistinguishable.

Because of the overwhelming similarities between the pyrimidine binding sites of the three classes of DHODs, it would seem that the orotate binding site is a poor target for the design of species-specific DHOD inhibitors. Despite this, two specific inhibitors, 3,4-dihydroxybenzoate (3,4-diOHB) and 3,5-dihydroxybenzoate (3,5-diOHB), were found to effectively inhibit Class 1A DHODs, while not affecting Class 1B or Class 2 DHODs (*11*). The origin of this selectivity has been a mystery, given the nearly identical pyrimidine binding sites in each class of DHOD. To address this enigma, the mechanism of ligand binding to the Class 1A DHOD from *Lactococcus lactis* has been studied in detail by titrations, kinetics, and crystallography. Our results elucidate important features of protein−ligand recognition and the structural and functional differences between the different classes of dihydrooroate dehydrogenases that may prove important in drug design.

EXPERIMENTAL PROCEDURES

Materials. The wild-type Class 1A *L. lactis* DHOD and the Cys130Ser and Cys130Ala mutants were expressed in *Escherichia coli* and purified as described (*1*, *12*). All chemicals were from Sigma-Aldrich Chemical Co. except for 5-fluoroorotic acid, which was from Diagnostic Chemicals Limited.

Spectroscopic Titrations. Ligand dissociation constants were determined by adding concentrated aliquots of ligand to 1.00 mL solutions of enzyme and recording the flavin absorbance spectrum from 800 to 300 nm. Absorbance spectra were recorded using a Shimadzu UV-2501PC spectrophotometer. Temperature was maintained at 25 °C with a Peltier temperature control. Titrations were performed in the following buffers: 50 mM citrate for pH 6.0, 40 mM KP_i for pH values from 6.5 to 8.0, and 50 mM AMPSO for pH 8.5 and 9.0.

ITC. Isothermal titration calorimetry was performed with a Micro-Cal VP-ITC. Titrations were at 25 °C and pH 8.0 in either 50 mM Tris-Cl or 50 mM KP_i. Enzyme (∼100 μM) was titrated with concentrated 3,4-diOHB or 3,5-diOHB solutions that had been prepared in identical buffers. Data were analyzed using Origin 7.0 (OriginLab Corp.).

Kinetics. Stopped-flow studies were conducted using either a Hi-Tech SF-61DSX2 controlled by KinetAsyst 3 for Windows or a Hi-Tech SF-61 system controlled by the Macintosh program KISS (Kinetic Instruments, Inc.). Kinetic studies were performed at 4 °C. Binding kinetics of the wild-type enzyme were studied using the following buffers: 50 mM KP_i at pH 6.0 and pH 6.5; 40 mM KP_i or 0.1 M K^+ HEPES, at pH 7.5; and 0.1 M Tris HCl at pH 8.0. For the mutant enzyme, 0.1 M MOPS at pH 7.5 and 0.1 M CHES at pH 9.0 were used. Reaction traces were fit to a single-exponential plus a constant in order to determine values of observed rate constants, using either KinetAsyst 3 (Hi-Tech Scientific, Ltd.), pro Fit (Quantum Soft), or KISS.

Crystallization. Hanging drops of 2 μL of protein solution (17 mg/mL containing 2.6 mM 3,4-diOHB or 3,5-diOHB) and 2 μL of reservoir solutions were equilibrated over 1 mL of reservoir solution at room temperature. In the presence of 3,4-diOHB, green crystals appeared after 2 to 4 days in 30% PEG 6000, 1 mM DTT, 0.2 M sodium acetate, and 0.1 M Tris-Cl at pH 8.5. The light-orange crystals of the complex with 3,5-diOHB also appeared after 2 to 4 days using similar conditions, except that the buffer was at pH 8.8.

Collection of Diffraction Data. Diffraction data were measured to 2.3 and 2.0 Å resolution for the 3,4-diOHB and the 3,5-diOHB complexes, respectively. Data were collected using an in-house MAR 345 imaging plate detector from MAR Research with a rotating anode CuKα X-ray source from Rigaku operating at 80 kV and 50 mA. The crystals were flash-cooled to 120 K in mother liquor supplemented with 10% glycerol before data collection. Auto indexing, data reduction, and scaling were performed with programs from the HKL suite (*13*). The two complexes crystallize in the same monoclinic space group $P2_1$(Table 1). They have virtually identical cell constants (Table 1) that are comparable to those observed in the other structures of the enzyme (*14*, *12*). The asymmetric unit contains the DHOD A homodimer corresponding to 54% solvent. The structures were refined in REFMAC5 (*15*) using the K136E mutant structure of *L. lactis* DHOD A (pdb code 1OVD (*14*)) without water molecules or orotate as the initial model. Density in the active sites revealed the position of the bound inhibitors and acetate ions. Water molecules were picked with ARP-wARP (*16*). Model building was done using O (*17*). Details of diffraction data and refinement are summarized in Table 1.

RESULTS

Spectral Titrations. The binding of ligands to the active site of DHOD causes significant perturbations to the flavin absorbance spectrum, allowing dissociation constants to be measured by titration. The pH dependence was determined for the binding of 3,4-diOHB, 3,5-diOHB, orotate, 5-fluoroorotate, and oxonate (4,6-dihydroxy-1,3,5-triazine-2-carboxylate) from pH 6 to pH 9 (see Chart 1 for structures). When 3,4-diOHB was bound, a new absorbance band appeared at 640 nm indicating that a charge-transfer complex was formed, while the other four ligands caused red shifts in the flavin spectrum that were similar to shifts reported previously (*1*, *4*, *10*, *11*, *14*). The absorbance changes as a function of the ligand concentration were fit to a hyperbola in order to determine the K_D. Absorbances at wavelengths giving the largest changes were used: 640 nm for 3,4-diOHB, 508 nm for 3,5-diOHB, 511 nm for orotate, 511 nm for 5-fluoroorotate, and 506 nm for oxonate.

Table 1: Diffraction Data and Refinement Statistics

	3,4-diOHB complex	3,5-diOHB complex
	diffraction data	
X-ray source	CuKa, in-house	CuKa, in-house
wavelength (Å)	1.54179	1.54179
resolution (Å)[a]	25 − 2.3 (2.41 − 2.32)	25 − 2.0 (2.08 − 2.03)
space group	$P2_1$	$P2_1$
cell parameters	$a = 53.6$ Å, $b = 108.2$ Å, $c = 66.2$ Å, $\beta = 104.1°$	$a = 53.7$ Å, $b = 108.1$ Å, $c = 66.2$ Å, $\beta = 104.1°$
R merge (%)[b]	5.8 (23.1)	7.8 (33.7)
no. of reflections	186529	184151
no. of unique reflections	32557	47526
$I/\sigma(I) > 2$ (%)	22.9 (5.6)	21.5 (6.3)
completeness (%)	90.6 (62.8)	93.1 (47.5)
	refinement	
resolution	25 − 2.3 (2.36 − 2.3)	25 − 2.04 (2.093 − 2.04)
no. of atoms	5068	5178
no. of reflections in test set	1526 (5.2%)	2236 (5.1%)
no. of reflections in working set	27913 (94.8%)	41966 (94.9%)
no. of reflections in total	29439	44202
average *B*-factor (Å^2)	36.1	28.5
R-factor (%)[c]	18.6 (25.0)	18.4 (29.4)
R free (%)[d]	24.0 (30.4)	22.9 (28.3)

[a] Values in parentheses are data for the highest resolution shell. [b] $R_{merge} = \Sigma|I - \langle I\rangle|/\Sigma I$, where the sums are over all reflections of intensity *I*. [c] $R_{factor} = \Sigma_{work}||F_{obs}| - k|F_{calc}||/\Sigma_{work}F_{obs}$ [d] $R_{free} = \Sigma_{test}||F_{obs}| - k|F_{calc}||/\Sigma_{test}F_{obs}$, where F_{obs} and F_{calc} are observed and calculated structure factors, respectively, *k* is the scale factor, and the sums are the overall reflections in the working set and test set, respectively.

Chart 1: Structures of Ligands Used in Binding Experiments

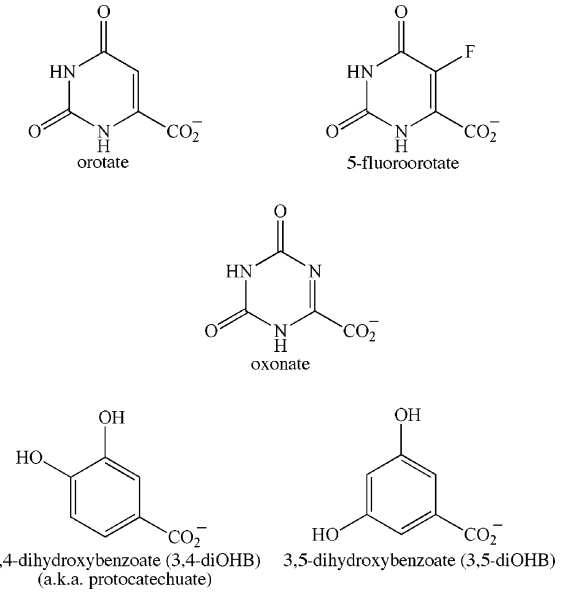

The strength of binding of three of the five ligands investigated varied with pH (Figure 1), indicating that the ionization of groups on the enzyme or the ligand, or both, caused important changes in protein−ligand interactions. The K_D of 3,4-diOHB increased as pH decreased, indicating that protonating one or more groups weakens 3,4-diOHB binding. There was no sign of a plateau in the K_D as the pH decreased, nor was there a sign of an inflection point, which would indicate the approach to a finite K_D at low pH. Therefore, within the experimentally available pH range, the data are consistent with binding only after a group on either the enzyme or 3,4-diOHB is deprotonated. The variation of K_D with pH in such a model is described by eq 1. In eq 1, K_D^{high} is the dissociation constant of the fully deprotonated species whose ionization is described by pK_a. The pK_a controlling 3,4-diOHB binding, obtained by fitting to eq 1, was ~6.8 (an uncertain value because it is at the low end of the pH range examined), and the value of K_D^{high} was 29 ± 3 μM[2].

$$K_D = K_D^{high}(1 + 10^{pK_a - pH}) \quad (1)$$

The K_D values for both 3,5-diOHB and 5-fluoroorotate increased somewhat at pH values above 8, suggesting that one or more deprotonations weaken their binding. The pK_a values controlling the binding of 3,5-diOHB and 5-fluoroorotate were greater than 9, making them too high to measure. In contrast to this behavior, the K_D values for orotate and oxonate did not change significantly with pH, suggesting that groups interacting with these two ligands do not deprotonate from pH 6 to pH 9. Alternatively, two ionizations could have counterbalancing affects, with one weakening binding and the other strengthening it, causing no change to the K_D. Oxonate has a pK_a of 6.9 (*41*), a value within the range of these experiments, perhaps suggesting that this ionization might be compensated by that of an enzymatic group resulting in no net change in binding strength, but the identity of such an enzymatic group is not apparent.

The binding of 3,4-diOHB to the Cys130Ser and Cys130Ala mutants was also studied. These mutant enzymes also formed charge-transfer complexes upon binding 3,4-diOHB, but the maxima of the broad charge-transfer bands were shifted to shorter wavelengths: 610 nm for Cys130Ser and 590 nm for Cys130Ala. The strength of binding was dependent on pH (Figure 1). At high pH values, the K_D^{high} for the Cys130Ser mutant (61 ± 7 μM) was slightly higher than that found for the wild-type enzyme. At lower pH values, binding weakened. The pH dependence of the K_D was fit to

[2] Equation 1 does not predict an inflection point in the pH dependence of K_D despite intuitive expectations. This is because the value of K_D becomes infinite at low pH. However, the pH dependence of the *association* constant ($1/K_D$) will have an inflection point at the pK_a.

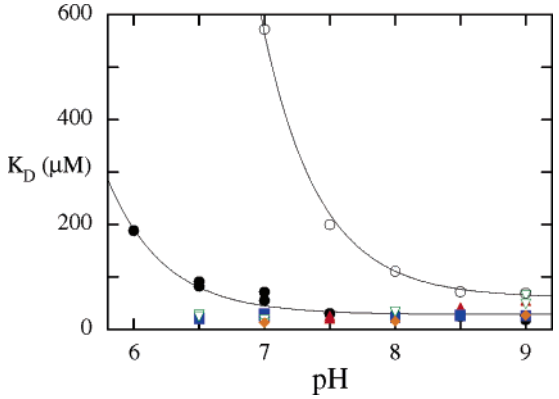

FIGURE 1: Dissociation constants as a function of pH. Dissociation constants of ligands were determined in spectral titrations of the wild-type and Cys130Ser enzymes at 25 °C as described in Experimental Procedures. For titrations of the wild-type enzyme, the ligands were 3,4-diOHB (filled black circles), 3,5-diOHB (filled, red, point-up triangles), orotate (blue squares), 5-fluoroorotate (open, green, point-down triangles), and oxonate (orange diamonds). The buffers used were 50 mM citrate for pH 6.0, 40 mM KPi for pH values ranging from 6.5 to 8.0, and 50 mM AMPSO for pH 8.5 and 9.0. The Cys130Ser mutant was titrated with 3,4-diOHB (open black circles) in 0.1 M MOPS at pH 7.0 and 7.5, 0.1 M Tris-Cl at pH 8.0 and 8.5, and 0.1 M CHES at pH 9.0 and 9.5. The variation of the K_D of 3,4-diOHB for the wild-type and mutant enzymes was fit to eq 1 (curves), giving apparent pK_a values of 6.75 ± 0.05 and 7.92 ± 0.06, respectively, and values of K_D^{high} of 29 ± 3 μM for wild-type and 61 ± 7 μM for Cys130Ser.

eq 1, suggesting that a group with a pK_a of 7.9 ± 0.1 must be deprotonated to allow binding. This pK_a value is about 1 unit higher than that observed for the wild-type enzyme. Binding of 3,4-diOHB to the Cys130Ala mutant was significantly weaker. Saturation was not achieved in titrations at pH values lower than 8.5. At pH 8.5 and 9.0, K_D values of 1.6 and 2.3 mM, respectively, were obtained.

Phenolate Absorbance. The possibility that ligands ionize upon binding was investigated by looking for changes in the absorbance spectrum associated with the deprotonated ligand. The ultraviolet absorbance of phenols shifts significantly to longer wavelengths upon deprotonation to the phenolate. The phenolic form of 3,4-diOHB absorbs maximally at 250 and 287 nm; these peaks shift to 276 and 299 nm upon formation of the phenolate. In titrations, most of this region of the absorbance spectrum is obscured by the high absorbance of the enzyme. However, a minimum in the enzyme absorbance from 300 to 310 nm provides a window for observing the edge of the phenolate peak, permitting the observation of phenolate formation. The formation of the phenolate absorbance band was observed at 310 nm (Figure 2A) when 3,4-diOHB was bound to the enzyme. When titrations were performed at pH values well below the pK_a of aqueous 3,4-diOHB (8.67 (*18*)), a hyperbolic increase in the absorbance at 310 nm was seen as binding occurred, followed by a linear increase in absorbance due to free ligand after saturation of the enzyme (Figure 2A). Thus, binding to DHOD A causes the phenolic pK_a of 3,4-diOHB to decrease so that the phenolate form is bound, implicating the phenolic oxygen of 3,4-diOHB as one of the ionizing groups that controls the strength of binding. In contrast, phenolate formation is not seen upon 3,5-diOHB binding; only a linear increase of absorbance at 310 nm is seen throughout titrations (Figure 2B), indicating that the enzyme does not stabilize the phenolate of 3,5-diOHB.

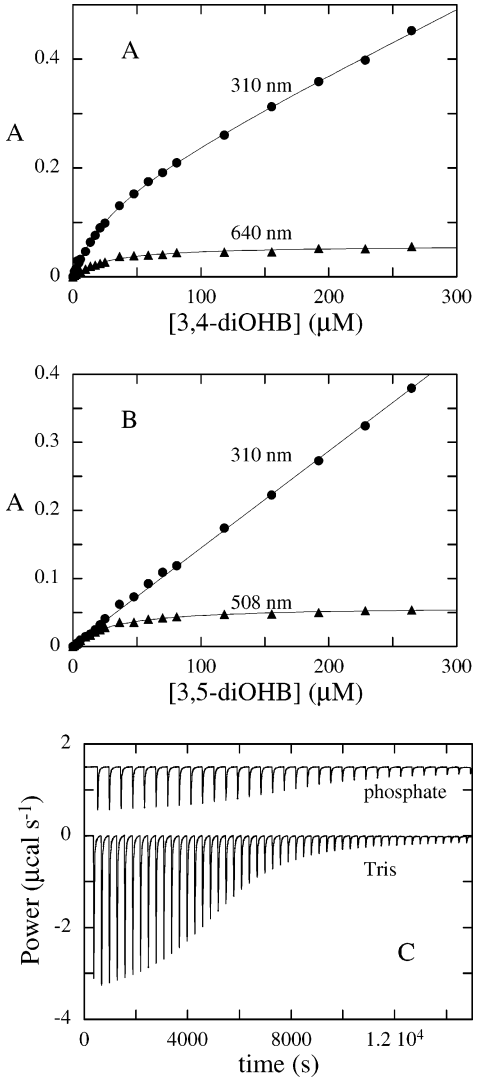

FIGURE 2: Observation of the phenolate of enzyme-bound 3,4-diOHB but not 3,5-diOHB by absorbance spectroscopy and ITC. (A) The increased absorbance caused by phenolate formation upon 3,4-diOHB binding was observed at 310 nm in spectral titrations of 19 μM enzyme at 25 °C, whereas the change in the flavin environment caused by the binding of this ligand was observed at 640 nm. Note that as the complex was being formed in the beginning of the titration, the absorbances at both wavelengths changed, but once the enzyme was saturated (>∼50 μM 3,4-diOHB), the absorbance at 640 nm stopped changing, while the phenolate absorbance increased as the unbound ligand concentration increased. (B) In contrast to the behavior in A, 3,5-diOHB did not form phenolate upon binding, as evidenced by the linear increase in absorbance at 310 nm throughout the whole titration. (C) The ionization of 3,4-diOHB was also detected calorimetrically. Enzyme solutions (112 μM) in either 50 mM Tris-Cl or 50 mM KP_i, both at pH 8.0 and 25°, were titrated with concentrated 3,4-diOHB in the same buffer. The large difference observed between the enthalpies in these titrations is due to the different enthalpies of the reaction of the buffer with the proton expelled upon ligand binding (Scheme 1).

Isothermal Titration Calorimetry. The conclusion that 3,4-diOHB binding is accompanied by deprotonation was investigated further by determining the buffer dependence of the enthalpy of binding using isothermal titration calorimetry (ITC). The titrations were performed in two different buffers: 50 mM Tris-Cl at pH 8.0 and 50 mM KP_i at pH 8.0. Binding was exothermic in both buffers (Figure 2C). However, the observed enthalpy depended on the identity

Scheme 1

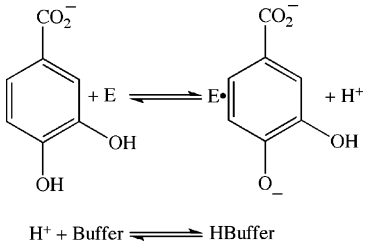

of the buffer. Binding in potassium phosphate gave −2.79 kcal mol^{-1}, while binding in Tris gave −8.72 kcal mol^{-1}. The difference can be attributed to the protonation of the buffer by the proton released from the enzyme−3,4-diOHB complex (Scheme 1 (*19*)); the enthalpies for protonating phosphate and Tris are +1 and +11.5 kcal mol^{-1}, respectively (*20*).

Kinetics of 3,4-diOHB Binding. The binding of 3,4-diOHB to the wild-type enzyme was studied at 4 °C by monitoring the formation of charge-transfer absorbance. Stopped-flow experiments were conducted by mixing enzyme (∼20 μM after mixing) with 3,4-diOHB (50 μM−4 mM after mixing). Binding was studied from pH 6.0, where it was relatively slow, to pH 8.0. Above pH 8, binding was too fast to measure. Absorbance traces, obtained at 640 nm, were single exponentials at all pH values investigated (Figure 3A). The observed rate constants increased hyperbolically with increasing 3,4-diOHB concentration (Figure 3B) to limiting values that depended on the pH. At all pH values, the intercepts extrapolated to essentially the same nonzero value (∼4 s^{-1}; Table 2) as the 3,4-diOHB concentration approached zero. The nonlinearity of the concentration dependence of k_{obs} requires that there be at least two reaction steps to produce the observed charge-transfer complex. A two-step binding scheme (Scheme 2) was used to analyze the data. In this mechanism, 3,4-diOHB (abbreviated P for protocatechuate, the trivial name of 3,4-diOHB) initially binds rapidly, followed by a slower isomerization step that generates charge-transfer absorbance.

If a rapid equilibrium is assumed for the first step, then the observed rate constant is given by eq 2 (*21*).

$$k_{obs} = k_b + \frac{k_a[3,4\text{-diOHB}]}{K_P + [3,4\text{-diOHB}]} \quad (2)$$

It was possible to fit the kinetics of binding obtained at each pH value to eq 1. The values of K_P and k_b did not vary systematically with pH (Table 2), giving average values of 940 ± 290 μM and 4 ± 1 s^{-1}, respectively (Figure 3C). In contrast, the value of k_a increased with pH (Figure 3C and Table 2). A plot of log k_a versus pH gave an apparent straight line with a slope of 0.7. This value is significantly lower than one, the theoretical value for an increase in rate constant far below a pK_a value. Linear pH dependences with nonintegral slopes are occasionally reported (*22*−*24*) and may be ascribed to the presence of two pK_a values that are close enough that a slope of 0.7 is obtained in the narrow pH range accessible to the experiment.

The analysis of the kinetic data by eq 2 allows the calculation of the overall thermodynamic K_D, the K_D obtained in titrations, which is a function of the equilibrium constants

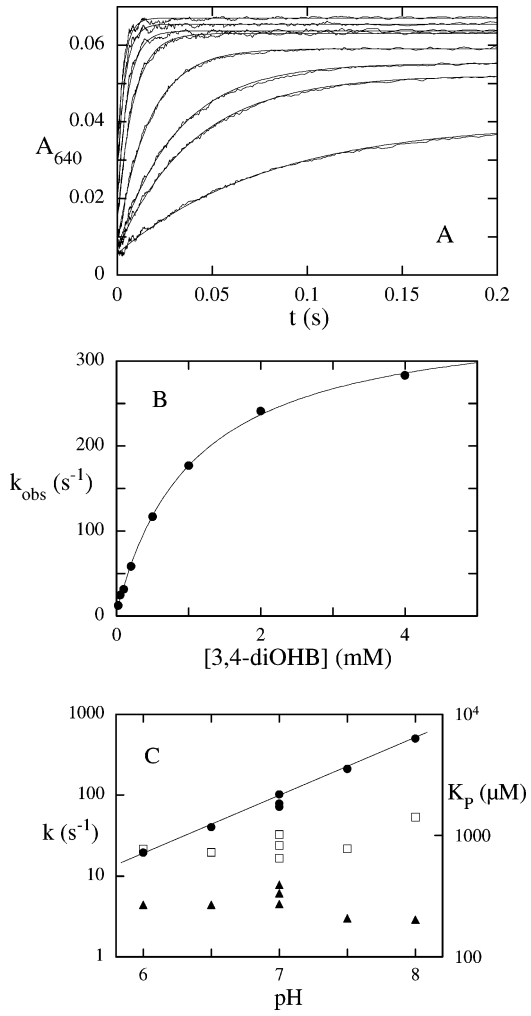

FIGURE 3: Kinetics of 3,4-diOHB Binding. Enzyme (17.0 μM after mixing) was mixed with 3,4-diOHB at 4 °C in a stopped-flow spectrophotometer and the formation of the charge-transfer complex was monitored at 640 nm. Panel A shows raw data obtained at pH 8.0. Panel B shows the variation with concentration of the observed rate constants obtained by single-exponential fits. The hyperbolic concentration dependencies were analyzed to obtain the initial dissociation constant K_P and the rate constants for isomerization to and from the charge-transfer complex, k_a and k_b, as described in the text. The variation of these parameters with pH is plotted in panel C. The rate constants for charge-transfer complex formation, k_a, are shown by filled circles. The rate constants for the reverse reaction, k_b, are shown by filled triangles. The values for the initial dissociation constants, K_P, are plotted as open squares.

of the first and second steps of the two-step binding reaction in Scheme 2. The dissociation constant and rate constants derived from the two-step kinetic analysis are related to the overall thermodynamic dissociation constant by

$$K_D = \frac{K_P K_{iso}}{1 + K_{iso}} \quad (3)$$

where

$$K_{iso} = \frac{k_b}{k_a} \quad (4)$$

The overall thermodynamic dissociation constant, K_D, was also obtained in the kinetic experiments from the variation of the total absorbance change with 3,4-diOHB concentration

Table 2: Rate and Dissociation Constants from Kinetic Experiments

pH	K_P (μM)	k_a (s^{-1})	k_b (s^{-1})	K_{iso}	$K_{D,obs}$ (μM)[a]	$K_{D,calc}$ (μM)[b]
6.0	780 ± 80	19.5 ± 0.7	4.4 ± 0.2	0.23 ± 0.02	113 ± 7	140 ± 20
6.5	730 ± 40	40.2 ± 0.5	4.4 ± 0.3	0.109 ± 0.009	89 ± 2	72 ± 9
7.0	833 ± 185	84 ± 16	6.1 ± 2	0.06 ± 0.01	50 ± 11	58 ± 11
7.5	780 ± 40	211 ± 3	3 ± 1.8	0.014 ± 0.009	8 ± 2	11 ± 7
8.0	1420 ± 90	500 ± 10	2.9 ± 2.6	0.006 ± 0.005	15 ± 1	8 ± 8

[a] Obtained from the half-saturating concentration of the absorbance change caused by binding. [b] Calculated from kinetic parameters using eq 3.

Scheme 2

$$E + P \overset{K_P}{\rightleftharpoons} C_P \underset{k_b}{\overset{k_a}{\rightleftharpoons}} C_T$$

after equilibrium had been established. Thus a check for self-consistency was possible by comparing the value of the K_D calculated from the kinetic analysis to that measured directly from absorbance changes. These values, listed in Table 2, show that good agreement was found at all pH values examined, providing support for the two-step mechanism in Scheme 2 and validating the assumption of rapid equilibrium binding.

Kinetics of Orotate and 3,5-diOHB Binding. When either orotate or 3,5-diOHB were mixed with the wild-type enzyme in stopped-flow experiments, the red shift of the flavin spectrum was nearly complete in the dead time, indicating that binding was too fast to observe directly. Therefore, competition experiments were done to study the kinetics of the dissociation of these ligands. The preformed enzyme−orotate complex (18 μM enzyme and 0.3 mM orotate before mixing) was mixed at pH 7.0 and 4 °C with 3,4-diOHB in concentrations varying between 1 and 25.6 mM (before mixing), as shown in Figure 4. Absorbance at 640 nm developed in a single exponential but more slowly than when orotate was absent. The observed rate constant increased hyperbolically with increasing 3,4-diOHB concentration to a limiting value of 28 s^{-1}. The intercept, as the 3,4-diOHB concentration approached zero, was 5.5 s^{-1}, essentially the same as the value of 4 s^{-1} found for the rate constant for the reverse isomerization of the 3,4-diOHB complex, k_b.

The reverse of the above competition reaction was also done by mixing the preformed enzyme−3,4-diOHB complex (18 μM enzyme and 0.4 mM 3,4-diOHB before mixing) with varying concentrations of orotate (between 0.04 and 5.12 mM before mixing), as seen in Figure 5. The observed rate constant decreased hyperbolically with increasing orotate concentration, to a limiting value of 4.5 s^{-1}, and an intercept of 24 s^{-1} was obtained when the orotate concentration approached zero. Note that these values are similar to those obtained in the competition experiments described above that started with the orotate complex.

The simplest mechanism compatible with the concentration dependencies in these competition experiments is a single-step binding/dissociation of orotate coupled to the two-step binding/dissociation of 3,4-diOHB, shown in Scheme 3, where L represents orotate and P represents 3,4-diOHB.

Expressions for the observed rate constants controlling the kinetics of the two competition experiments are derived in the Appendix. This analysis shows that the limiting value of the observed rate constant at saturating 3,4-diOHB in the experiment shown in Figure 4 is a function of the rate constant for orotate dissociation, k_{off}, and the forward and

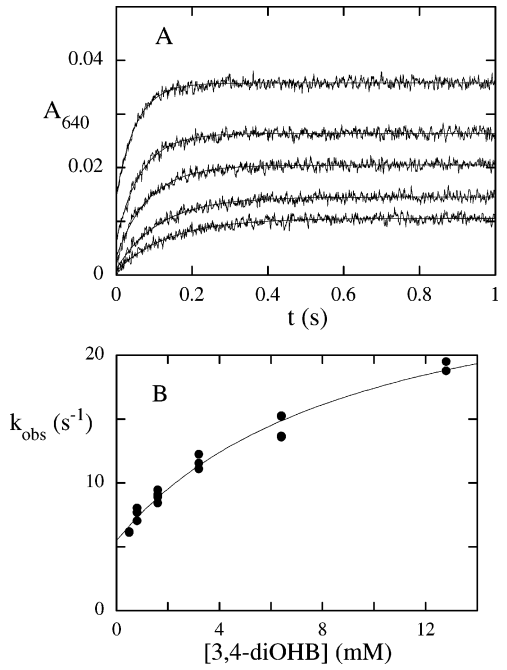

FIGURE 4: Dissociation kinetics of orotate by competition with 3,4-diOHB. The dissociation of orotate from the enzyme was observed by mixing the enzyme−orotate complex (18 μM enzyme and 0.3 mM orotate before mixing) with various concentrations of 3,4-diOHB at pH 7.0, 4 °C. Reaction traces monitoring charge-transfer complex formation (640 nm) are shown in panel A. The concentration dependence of the observed rate constants obtained from single-exponential fits is show in panel B.

reverse rate constants for the isomerization reaction between the initial 3,4-diOHB complex and the charge-transfer complex, k_a and k_b, respectively, which were obtained directly from the kinetics of 3,4-diOHB binding to the enzyme (Table 2). Thus, a value of k_{off} for orotate dissociation of 40 ± 9 s^{-1} was calculated. The analysis in the Appendix also allows the bimolecular rate constant k_{on} for orotate binding to be calculated from the half-saturating concentration of 3,4-diOHB in Figure 4 and the parameters in Table 2; a value of 9.1 ± 0.1 × 10^6 M^{-1} s^{-1} was obtained. The rate constants calculated for orotate binding are summarized in Table 3. The analysis in the Appendix also shows that the intercept of the observed rate constant as the concentration of 3,4-diOHB goes to zero should be k_b, found directly to be ∼4 s^{-1} (Table 2). The data in Figure 4 are consistent with this prediction. The opposite competition experiment, in which the enzyme−3,4-diOHB complex was mixed with orotate, is shown in Figure 5. The data obtained in this experiment were also consistent with Scheme 3. The analysis given in the Appendix predicts that the observed rate constant should approach k_b at high orotate; a limiting value of 4.5 s^{-1} was observed, in excellent agreement with other experiments.

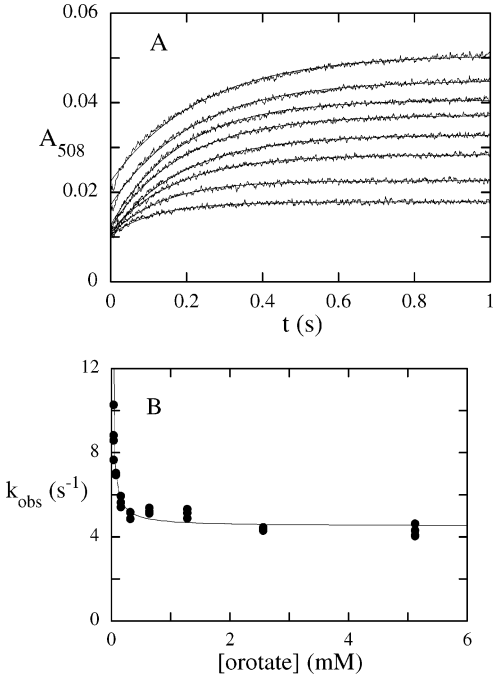

FIGURE 5: Dissociation kinetics of 3,4-diOHB by competition with orotate. The dissociation of 3,4-diOHB from the enzyme was studied by mixing the preformed complex (18 μM enzyme and 0.4 mM 3,4-diOHB before mixing) with various concentrations of orotate in a stopped-flow spectrophotometer at pH 7.0 and 4 °C. Traces obtained at 508 nm are shown in panel A. Panel B shows the variation of the observed rate constant with orotate concentration.

Scheme 3

$$C \underset{k_{on}}{\overset{k_{off}}{\rightleftharpoons}} E + L$$

$$E + P \underset{}{\overset{K_P}{\rightleftharpoons}} C_P \underset{k_b}{\overset{k_a}{\rightleftharpoons}} C_T$$

Competition experiments were also carried out with 3,5-diOHB. The preformed enzyme−3,5-diOHB complex (18 μM enzyme and 0.3 mM 3,5-diOHB before mixing) was mixed with 3,4-diOHB in varying concentrations between 0.05 and 3.2 mM (before mixing), as seen in Figure 6. The observed rate constant increased hyperbolically with increasing 3,4-diOHB concentration to a limiting value of 39 s^{-1} at high 3,4-diOHB and an intercept of 4 s^{-1} when the 3,4-diOHB concentration approached zero. The obverse experiment was also performed in which the enzyme−3,4-diOHB complex was mixed with 3,5-diOHB, with ligand exchange being observed at 510 nm. A limiting value for the observed rate constant of 4.5 s^{-1} was obtained at high 3,5-diOHB concentrations. As the concentration of 3,5-diOHB was lowered, the value of the observed rate constant increased. However, this occurred at concentrations too low to allow a meaningful extrapolation back to the intercept. These competition experiments are also explained by the model for orotate binding described above (Scheme 3, with L being 3,5-diOHB), giving a value of k_{off} for 3,5-diOHB of 65 ± 31 s^{-1} and a value for k_{on} of 4.3 ± 0.06 × 10^6 M^{-1} s^{-1} (Table 3).

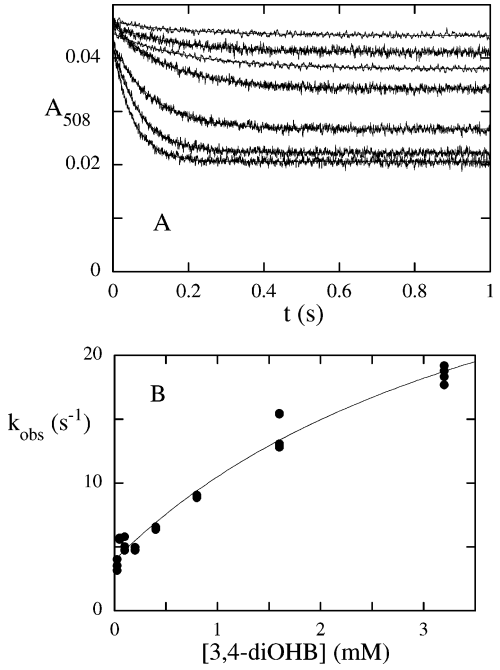

FIGURE 6: Dissociation kinetics of 3,5-diOHB by competition with 3,4-diOHB. The dissociation of 3,5-diOHB from the enzyme was studied by mixing the preformed complex (18 μM enzyme and 0.3 mM 3,5-diOHB before mixing) with various concentrations of 3,4-diOHB in a stopped-flow spectrophotometer at pH 7.0 and 4 °C. Panel A shows reaction traces obtained at 508 nm. Panel B shows the variation in the observed rate constant with the concentration of 3,4-diOHB.

Kinetics of Binding of 3,4-diOHB to Mutant Enzymes. Stopped-flow experiments were also performed with the Cys130Ser and Cys130Ala mutants in order to investigate the importance of the active site cysteine in binding 3,4-diOHB. At pH 9.0, 4°, the Cys130Ser mutant enzyme formed the charge-transfer complex with an observed rate constant that increased linearly with 3,4-diOHB concentration (Figure 7A). The slope of the dependence gave a bimolecular rate constant for association of 5.5 ± 0.04 × 10^5 M^{-1} s^{-1} and a dissociation rate constant of 23 ± 4 s^{-1}. The ratio of these rate constants gives a K_D of 42 ± 10 μM; the hyperbolic change in absorbance at 610 nm gave a K_D of 37 ± 3 μM, in excellent agreement with the value obtained from kinetics. Thus there is no evidence at this pH for a binding mechanism more complex than a single step. In contrast, when the experiment was performed at pH 7.5, the observed rate constant increased hyperbolically, with a limiting value of 419 ± 10 s^{-1} at high 3,4-diOHB concentration, an intercept of 22 ± 4 s^{-1} as 3,4-diOHB goes to zero, and a half-saturating concentration of 3,4-diOHB of 1.3 ± 0.1 mM (Figure 7B). These data require a two-step binding mechanism, similar to that of the wild-type enzyme. The apparent dissociation constant for the initial 3,4-diOHB complex and

Table 3: Rate Constants Describing the Binding of Orotate and 3,5-diOHB Obtained from Competition Experiments

ligand	$\lim_{L\to 0} k_{obs}$ (s^{-1})	$\lim_{L\to \infty} k_{obs}$ (s^{-1})	$P_{1/2}$ (mM)	k_{on} ($M^{-1}s^{-1}$)	k_{off} (s^{-1})
orotate	5.5 ± 0.4	29 ± 1	9.4 ± 2.2	9.1 ± 0.1 × 10^6	40 ± 9
3,5-diOHB	4.0 ± 1.0	39 ± 7	4 ± 0.3	4.3 ± 0.06 × 10^6	65 ± 31

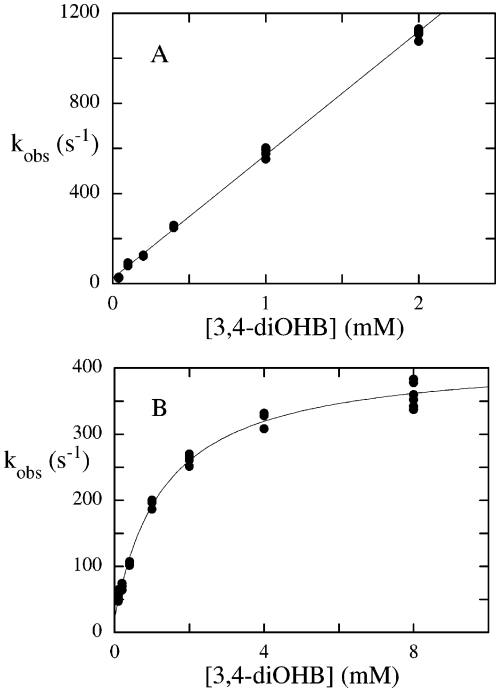

FIGURE 7: Kinetics of 3,4-diOHB binding to the Cys130Ser mutant. Stopped-flow experiments were performed at 4 °C to determine observed rate constants for the binding of 3,4-diOHB to the Cys130Ser mutant. A linear concentration dependence was observed when 0.1 M CHES at pH 9.0 was used (panel A), giving a bimolecular rate constant of $5.5 \pm 0.04 \times 10^5$ M^{-1} s^{-1} and a dissociation rate constant of 23 ± 4 s^{-1}. When 0.1 M MOPS at pH 7.5 was used as the buffer, a saturating increase in the observed rate constant was observed (panel B). Fitting to a hyperbola gave a maximum value of 419 ± 10 s^{-1}, an intercept of 22 ± 4 s^{-1} as the concentration of 3,4-diOHB approached zero, and a half-saturating concentration of 1.3 ± 0.1 mM.

both the forward and reverse isomerization rate constants are higher than those observed for the wild-type enzyme at pH 7.5 (Table 2). Although these values lead to slightly weaker overall binding and less charge-transfer complex at equilibrium, they also indicate that the mutation does not create a kinetic barrier to the formation of the charge-transfer complex. Similar experiments were also attempted with the Cys130Ala mutant. Unfortunately, binding was too rapid to be observed.

Structure Determination and Refinement. The crystal structures of the 3,4-diOHB and 3,5-diOHB complexes of the enzyme were determined from X-ray diffraction data. Rigid-body refinement with the two subunits of the dimer was performed, followed by cycles of positional refinement applying noncrystallographic symmetry (NCS) restraints on the two molecules (A and B) in the asymmetric unit. The difference electron density map showed the density matching the inhibitors in both complexes (Figure 8). After including the inhibitors in the models, a few rounds of positional refinement revealed that the inhibitors in both models were only bound in one subunit (B) of the dimer. In the active site of the other subunit (A), the difference electron density in both complexes was better interpreted as an acetate ion originating from the crystallization buffer. The active-site loop region in both models is more ordered in the subunit where the inhibitor was bound compared to the subunit with acetate bound. The NCS restraints were therefore not applied to the active site loop region (residues 128−140) of either subunit.

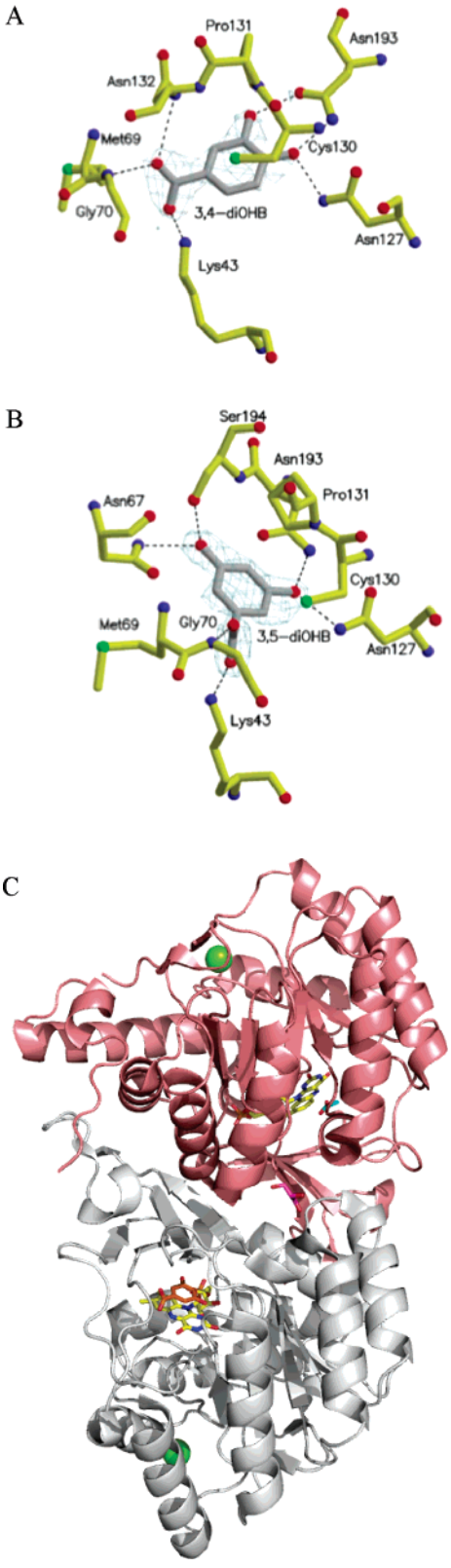

FIGURE 8: Structures of the 3,4-diOHB and 3,5-diOHB complexes. Panel A shows hydrogen bonds between 3,4-diOHB and the protein as well as difference electron density around the ligand contoured to 1.1σ level. The hydrogen bonds between the protein and 3,5-diOHB, and the electron density of that ligand are shown in a similar way in Panel B. Panel C shows the dimer of the 3,5-diOHB complex. Subunit A (salmon color) has an acetate ion (blue) bound near the flavin, whereas 3,5-diOHB (orange) occupies the active site of subunit B (white). The flavins of both subunits have yellow carbons. A Mg^{2+} ion (green sphere) is bound to each subunit, and a glycerol molecule (pink carbons) is bound between the subunits.

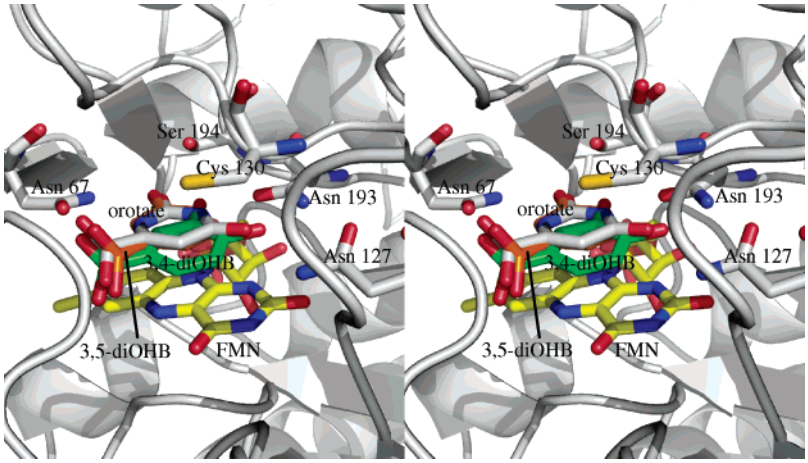

FIGURE 9: Stereoview of a comparison of the 3,4-diOHB, 3,5-diOHB, and orotate complexes. The structures of the 3,4-diOHB (pdb file 2BSL), 3,5-diOHB (pdb file 2BX7), and orotate (pdb file 2DOR) complexes were aligned by superimposing the isoalloxazine moieties of each structure. Only the flavin (yellow carbons) and the protein (white carbons) of the orotate complex (pdb file 2DOR) are shown for clarity, but those of the other complexes are virtually superimposable. Note that orotate (white carbons) and 3,5-diOHB (orange carbons) are also virtually superimposable, but 3,4-diOHB (green carbons) binds in a significantly different orientation.

As previously observed in the high-resolution structure of Arg57Ala DHOD A (*14*), there is density corresponding to a metal ion coordinated by six water molecules close to the C-terminal end of α-helix 1 in both complexes. The metal−ligand distances suggest that the metal ion is either sodium or magnesium, and the latter ion, assumed to originate from the pool of magnesium in the cell, was introduced in the model. One glycerol molecule from the cryoprotectant was located in both complexes at the interface between subunit A and B in a manner similar to Arg57Ala DHOD A (*14*). This glycerol molecule is surrounded by Tyr 141, His 173, and Phe 169 from each subunit. The final model of the 3,4-diOHB complex contains a total of 165 water molecules, whereas the model of the 3,5-diOHB complex contains 275 water molecules. Both subunits of both the 3,4-diOHB and 3,5-diOHB complexes contain all 311 amino acids, one FMN molecule, and one Mg^{2+} ion. Subunit A contains one acetate molecule, and subunit B has one inhibitor molecule bound. An overall picture of the 3,5-diOHB complex with bound cofactors, metal ions, and other ligands is shown in Figure 8C.

The final models have an *R*-factor of 18.6% (*R*-free 24.0%) and 18.4% (*R*-free 22.9%) for the 3,4-diOHB complex and the 3,5-diOHB complex, respectively. PROCHECK (*25*, *26*) and WHATIF (*27*) were used to check the quality of the final structures. The Ramachandran plot for the A-chain revealed that the 3,4-diOHB complex has 90.2% of the residues located in the most favored regions and 9.8% in the additionally allowed regions; for the B-chain, 89.4% of the residues were located in the most favored regions and 10.6% in the additionally allowed regions. The 3,5-diOHB complex has 92.8% and 93.2% residues located in the most favored regions and 7.2% and 6.8% in the additionally allowed regions for chain A and B, respectively. No residues appear in the disallowed regions for either complex. A summary of refinement statistics for the two structures is listed in Table 1.

Active-Site Interactions. The overall structures of both enzyme−inhibitor complexes were virtually identical to the structures previously reported for the free enzyme and the orotate complex (*5*, *28*). The mobile loop that shields the active site from solvent and opens to allow ligand exchange (*28*) was closed in both the 3,4-diOHB and 3,5-diOHB complexes. 3,5-diOHB adopts an orientation similar to that of orotate (Figure 9). The carboxylate group of 3,5-diOHB forms hydrogen bonds with the side chain of Lys 43 and the backbone NH groups from Gly 70 and Leu 71. The phenolic oxygen atoms of this ligand form hydrogen bonds with Asn 67, Asn 127, and Asn 193 in a fashion similar to that seen with the carbonyl oxygens of orotate. However, rotation of the amide groups of Asn 67 and either Asn 193 or Asn 127 relative to the orotate complex is required to fulfill hydrogen-bonding donor−acceptor criteria.

Interestingly, the orientation of 3,4-diOHB is very different from that of 3,5-diOHB or orotate. While the carboxylate group still forms hydrogen bonds to Lys 43, Met 69, Gly 70, and Leu 71, the ring of the molecule has rotated by 23° so that the phenolic oxygen at the 4-position forms hydrogen bonds with Asn 127 and Asn 193, with distances of 2.7 and 2.5 Å, respectively (Figure 10A). In addition to the hydrogen bond formed with the 4-OH of 3,4-diOHB by the amide nitrogen of the side chain of Asn 193, the carbonyl oxygen of this side chain forms a hydrogen bond with the 3-OH group, with a distance of 2.7 Å between oxygens. Unlike orotate, the ring of 3,4-diOHB does not interact with the side chain of Asn 67, whose closest distance is 4.6 Å. Some of the hydrogen-bond distances in the 3,4-diOHB and 3,5-diOHB complexes are compared to those of the orotate complex in Table 4.

DISCUSSION

The thermodynamic, kinetic, and structural data presented here allow for a detailed mechanism for 3,4-diOHB binding to DHOD A to be proposed. The ITC and spectral titrations provide good evidence that 3,4-diOHB loses a proton to bind as the phenolate. The stopped-flow experiments show that binding to the wild-type enzyme occurs with two steps (minimally), with the second step corresponding to the formation of the phenolate. The crystal structure shows that in the final complex, 3,4-diOHB, though stacked with the isoalloxazine ring system (Figure 9), is oriented differently relative to the orientation of orotate, allowing it to form

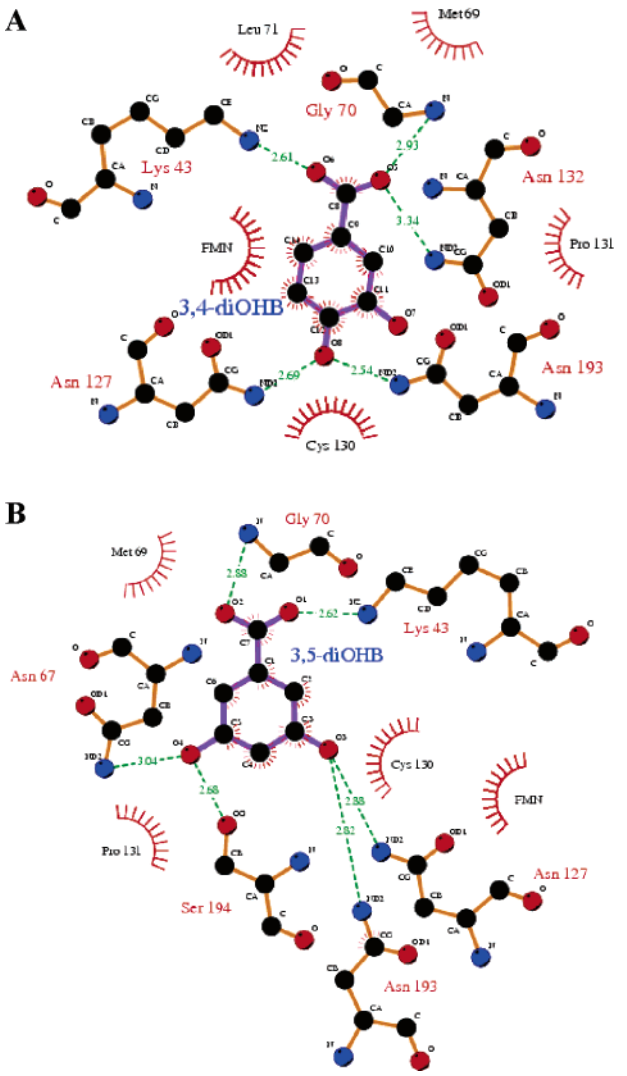

FIGURE 10: Ligand−protein interactions in the 3,4-diOHB and 3,5-diOHB complexes. The interactions between the enzyme and the dihydroxybenzoate ligands are shown in LIGPLOT diagrams. 3,4-diOHB is shown in A and 3,5-diOHB is shown in B.

Table 4: Summary of Selected Side Chain Ligand Hydrogen-Bond Distances[a]

	Distance from Protein Donor to Ligand Acceptor (Å)		
residue	OH of 3,4-diOHB[b]	OH of 3,5-diOHB[c]	C=O of orotate[d]
Asn 67	5.4	3.1	3.2
Asn 127	2.7	2.9	2.9
Asn 193	2.5 and 2.7[e]	2.9	2.9
Ser 194	3.5	2.7	2.8

[a] Distances are between heavy atom donor atoms from active-site side chains (N for Asn and O for Ser) and the closest acceptor oxygens of the ligands. [b] From PDB file 2BSL. [c] From PDB file 2BX7. [d] From PDB file 2DOR. [e] Assigned to the distance between the amide oxygen of the side chain and the 3-OH of 3,4-diOHB.

hydrogen bonds with Asn 127 and Asn 193 with ~2.5−2.7 Å O−N distances. This suggests that the enzyme lowers the pK_a of bound 3,4-diOHB by stabilizing the deprotonated state with very favorable hydrogen bonds. The two-step formation of the 3,4-diOHB charge-transfer complex observed kinetically suggests that initially, 3,4-diOHB binds rapidly in an orientation similar to that seen for orotate and 3,5-diOHB. Although the ligand is anchored by the hydrogen bonds to the carboxylate in this conformation, its binding is weak because the phenolic oxygens in this orientation are unable to make energetically favorable hydrogen bonds with the Asn side chains of the active site. In particular, the 4-OH would clash sterically with the amide oxygen of Asn 193. Favorable hydrogen bonds subsequently form with Asn 127 and Asn 193 once 3,4-diOHB rotates by ~23° and a phenolic oxygen, presumably the 4-OH, on the basis of the distances of hydrogen-bonding partners (Table 4), deprotonates to the phenolate, resulting in the green charge-transfer complex.

The mechanism of deprotonation of 3,4-diOHB is not clear. Bound ligands are shielded from solvent by a protein loop that closes over the active site, suggesting that direct deprotonation by water or buffer is not possible in this closed conformation. Cys 130, the active-site base, is located on this loop and could conceivably deprotonate the phenolic oxygen of 3,4-diOHB, though slowly because its position is not optimal. However, the Cys130Ser and the Cys130Ala mutant enzymes still rapidly form charge-transfer complexes with 3,4-diOHB, suggesting that the active site base does not deprotonate the phenol and that there is another mechanism. Interestingly, the pK_a that controls binding shifts upward by one unit when the active-site base was mutated to Ser and even further when the base was mutated to Ala, even though residue 130 does not touch the 4-OH of 3,4-diOHB, suggesting that the mutation causes a broader change in the environment of the 4-OH, which disfavors ionization. It is conceivable that the mutations favor the open conformation of the loop that shields the active site from solvent, although there is no obvious reason why the mutation should alter the loop conformation. This loop has high temperature-factors in all structures of the Class 1A DHOD from *L. lactis*, suggesting that the loop can be mobile (*5*, *14*, *28*). If the loop were open, then exposing the interactions of the 4-OH of 3,4-diOHB with Asn 127 and Asn 193 to solvent would weaken the hydrogen bonds and increase the phenolic pK_a, as apparently happens in the Cys130Ser mutant. Transient access to the active site when the loop is open could provide a possible pathway for deprotonation of 3,4-diOHB.

In contrast to the behavior of 3,4-diOHB, 3,5-diOHB binds in the phenolic form. The structure of the 3,5-diOHB complex shows that this ligand binds to the enzyme in a conformation that is essentially the same as that of orotate, though it requires the rotation of two Asn side chains to form hydrogen-bond interactions (Figure 9). Both 3,5-diOHB and orotate bind to the enzyme too rapidly to directly observe the reactions in stopped-flow experiments. There was no evidence from competition experiments for more than one step in the binding of these ligands. This is consistent with the notion that 3,5-diOHB and orotate bind directly in the orientation seen in the crystal structures. Interestingly, unlike 3,4-diOHB, 3,5-diOHB does not form a charge-transfer interaction in its complex, although it stacks with the isoalloxazine of FMN. This may be due to the poor orbital overlap when 3,5-diOHB is bound, its poorer ability to act as a donor when bound as the phenol, or the operation of both effects. Thus, DHOD A behaves in a fashion similar to that of other flavoproteins such as old yellow enzyme toward phenolic ligands: ionization to the phenolate is a requirement for a charge-transfer interaction (*29*).

While a detailed picture of ligand binding to DHOD A is emerging, the reason that 3,4-diOHB and 3,5-diOHB do not bind to Class 1B or Class 2 enzymes (*11*) is not obvious. Attempts were made to detect the binding of 3,4-diOHB and 3,5-diOHB to the Class 2 DHOD from *E. coli*. Even at concentrations of 0.1 M, no ligand binding could be detected by absorbance spectroscopy. If a detection limit of 5% complex formation is assumed (and our detection is likely to be more sensitive), then a lower limit of ~2 M is placed on the K_D of 3,4-diOHB for the *E. coli* DHOD. This is at least 5 orders of magnitude weaker than the binding of 3,4-diOHB to DHOD A or a minimum difference in affinities of 7 kcal mol^{-1}. This is a remarkable degree of discrimination for binding sites whose structures are so similar. It is puzzling that this discrimination is not observed with orotate, which binds with similar affinities to both Class 1A and Class 2 enzymes. Orotate interacts with analogous side chains in the active sites of the Class 1A DHOD from *L. lactis* and the Class 2 DHOD from *E. coli*, as might be expected from the similarities between the pyrimidine binding sites of these enzymes. The enigma, then, is how Class 2 DHODs discriminate between ligands such as orotate and 3,5-diOHB, which the Class 1A DHOD treats as congruent.

Given the similarities of the active sites in the different classes of DHOD enzymes, we have looked for other structural differences. The various classes of DHODs differ by their oligomeric states. The Class 1A enzymes are homodimers, the Class 1B heterotetramers, and the Class 2 enzymes are monomers. It is noteworthy that the two active sites of the homodimeric DHOD A differ in the crystal structures, with one subunit containing an inhibitor and the other an acetate ion. This illustrates cooperativity between the subunits, which was also indicated from kinetic studies (*30*). It is not obvious how subunit interactions in Class 1A DHODs could promote the binding of dihydroxybenzoates that do not bind to other classes of DHODs. Perhaps the oligomeric state could influence the mobility of the loop covering the active site, which is most exposed in the Class 1A enzymes.

The inability of the Class 1A pyrimidine binding site to discriminate between ligands could be a consequence of important functional/catalytic differences between the Class 1A enzymes and the Class 1B and Class 2 enzymes. Class 1A DHODs lack a separate binding site for the oxidizing substrate; fumarate apparently reacts at the pyrimidine binding site, which is vacated after the reductive half-reaction. In contrast, NAD^+, the electron acceptor for Class 1B enzymes, binds to the PyrK subunit in the heterotetrameric enzyme, and the respiratory quinones that are the natural electron acceptors for the Class 2 DHODs bind in a separate domain. Thus the pyrimidine binding sites of the Class 1B and Class 2 DHODs were free to evolve higher selectivities than the pyrimidine binding site of the Class 1A DHODs, which is constrained to also accommodate fumarate. Unfortunately, the mechanistic and structural data currently available do not allow us to understand why these sites differ in their ligand selectivity.

Regardless of the origins of class-specific binding of dihydroxybenzoate, the ability to specifically inhibit Class 1A DHODs may ultimately lead to useful drugs. Class 1A DHODs are found in many Gram-negative bacteria and in some microbial eukaryotes. Several of the organisms that express Class 1A DHODs, such as *Enterococcus faecalis* and trypanosomes, cause diseases. Many of the bacteria that express Class 1A DHODs also express Class 1B enzymes (*3*, *31*). Data are emerging that suggest that the reduction of fumarate by Class 1A enzymes during anaerobic growth might be a more important function than pyrimidine synthesis (*32*−*34*). Thus, even if redundant DHODs allow pyrimidine synthesis in the presence of an inhibitor of Class 1A DHODs, the inhibitor could still be toxic. Consequently, there is growing interest in determining structures of other Class 1A DHODs (*35*, *36*) and developing inhibitors (*33*, *37*, *38*). Interestingly, inhibition by dihydroxybenzoates appears to be a general phenomenon in this class of enzymes (*33*). The affinities of the dihydroxybenzoates are not extremely high, but 3,4-diOHB and 3,5-diOHB bind tighter than the substrate DHO by 1 order of magnitude, suggesting that they might be promising lead compounds in the development of more potent inhibitors. Understanding the detailed mechanism of dihydroxybenzoate binding should facilitate this effort.

ACKNOWLEDGMENT

We gratefully acknowledge the help of Professor David P. Ballou and the late Professor Vincent Massey, University of Michigan, for the use of their stopped-flow spectrophotometers, and we thank Professor Raymond Trievel, University of Michigan, for the use of the isothermal titration calorimeter, and Professor Kaj Frank Jensen, University of Copenhagen, for supplying expression plasmids. We thank Flemming Hansen for help with the X-ray data collection.

APPENDIX

Analysis of Competitive Binding Kinetics Using a Ligand with a Two-Step Binding Mechanism. The determination of the rate constant for the dissociation of a ligand from a complex by competition with another ligand is well known for the simple case in which the competing ligand binds in one step (*39*). In this study, 3,4-diOHB, which binds in two steps, was used as a competing ligand. The analysis of two types of experiments involving a two-step competitor is presented in this Appendix.

After the preformed enzyme−orotate or 3,5-diOHB complex (abbreviated C) is mixed with a large excess of 3,4-diOHB (abbreviated P for protocatechuate, the trivial name of 3,4-diOHB), orotate or 3,5-diOHB (abbreviated L) dissociates in a single step, and the free enzyme (E) binds P to give the initial complex (C_P), which isomerizes to the charge-transfer complex (C_T). This is summarized in Scheme A1.

The first step in the binding of P is a rapid equilibrium, allowing Scheme A1 to be replaced with the equivalent Scheme A2 (*40*) where E′ represents the rapidly equilibrating enzyme forms E and C_P. In this Scheme, the rate constants k'_a and k'_{on} are the rate constants k_a and k_{on} modified by the fraction of E′ in the forms that are capable of reacting (eqs A1 and A2).

$$k'_a = \frac{k_a P}{K_P + P} \tag{A1}$$

$$k'_{on} = \frac{k_{on} K_P L}{K_P + P} \tag{A2}$$

Scheme A1

$$C \underset{k_{on}}{\overset{k_{off}}{\rightleftharpoons}} E + L$$

$$E + P \underset{}{\overset{K_P}{\rightleftharpoons}} C_P \underset{k_b}{\overset{k_a}{\rightleftharpoons}} C_T$$

Scheme A2

$$C \underset{k'_{on}}{\overset{k_{off}}{\rightleftharpoons}} E' \underset{k_b}{\overset{k'_a}{\rightleftharpoons}} C_T$$

Scheme A3

$$C_T \underset{k_b}{\overset{k_a}{\rightleftharpoons}} C_P \overset{K_P}{\rightleftharpoons} E + P$$

$$E + L \underset{k_{on}}{\overset{k_{off}}{\rightleftharpoons}} C$$

Scheme A4

$$C_T \underset{k'_a}{\overset{k_b}{\rightleftharpoons}} E' \underset{k_{off}}{\overset{k'_{on}}{\rightleftharpoons}} C$$

The steady-state solution describing Scheme A2 gives the observed rate constant for the formation of C_T (eq A3) (*21*).

$$k_{obs} = \frac{k_{off}k'_a + k'_{on}k_b + k_{off}k_b}{k_{off} + k'_{on} + k'_a} \tag{A3}$$

Substituting eqs A1 and A2 into A3 and simplifying gives the dependence of k_{obs} on the concentration of P.

$$k_{obs} = \frac{\left(\frac{k_{on}L + k_{off}}{k_{off} + k_a}\right)k_bK_P + \left(\frac{k_a + k_b}{k_{off} + k_a}\right)k_{off}P}{\left(\frac{k_{on}L + k_{off}}{k_{off} + k_a}\right)K_P + P} \tag{A4}$$

The hyperbolic concentration dependence is described by the half-saturating concentration of P ($P_{1/2}$) and by the limits at high and low P and (eqs A5−A7).

$$\lim_{P\to 0} k_{obs} = k_b \tag{A5}$$

$$\lim_{P\to\infty} k_{obs} = \left(\frac{k_a + k_b}{k_{off} + k_a}\right)k_{off} \tag{A6}$$

$$P_{1/2} = \left(\frac{k_{on}L + k_{off}}{k_{off} + k_a}\right)K_P \tag{A7}$$

When k_a, k_b, and K_P are available independently, as in this work from the direct analysis of the kinetics of 3,4-diOHB binding, k_{on} and k_{off} can be obtained from competition experiments.

The opposite competition experiment, in which preformed C_T is mixed with L, may be analyzed in a similar way. The experiment is described by Scheme A3; applying the rapid equilibrium assumption gives the equivalent Scheme A4, with k'_a and k'_{on} still being defined in eqs A1 and A2.

The steady-state solution (eq A8) gives k_{obs} as a function of L.

$$k_{obs} = \frac{\left[\frac{k_bK_P + (k_a + k_b)P}{k_{on}K_P}\right]k_{off} + k_bL}{\frac{k_bK_P + (k_a + k_b)P}{k_{on}K_P} + L} \tag{A8}$$

The limiting behavior and half-saturating concentration are given in eqs A9−A11.

$$\lim_{L\to 0} k_{obs} = k_{off} \tag{A9}$$

$$\lim_{L\to\infty} k_{obs} = k_b \tag{A10}$$

$$L_{1/2} = \frac{k_bK_P + (k_a + k_b)P}{k_{on}K_P} \tag{A11}$$

REFERENCES

1. Björnberg, O., Rowland, P., Larsen, S., and Jensen, K. F. (1997) Active site of dihydroorotate dehydrogenase A from *Lactococcus lactis* investigated by chemical modification and mutagenesis, *Biochemistry 36*, 16197−16205.
2. Nagy, M., Lacroute, F., and Thomas, D. (1992) Divergent evolution of pyrimidine biosynthesis between anaerobic and aerobic yeasts, *Proc. Natl. Acad. Sci. U.S.A. 89*, 8966−8970.
3. Nielsen, F. S., Anderson, P. S., and Jensen, K. F. (1996) The B form of dihydroorotate dehydrogenase from *Lactococcus lactis* consists of two different subunits, encoded by the pyrDb and pyrK genes, and contains FMN, FAD, and [FeS] redox centers, *J. Biol. Chem. 271*, 29359−29365.
4. Björnberg, O., Grüner, A. C., Roepstorff, P., and Jensen, K. F. (1999) Activity of *Escherichia coli* dihydroorotate dehydrogenase is dependent on a conserved loop identified by sequence homology, mutagenesis, and limited proteolysis, *Biochemistry 38*, 2899−2908.
5. Rowland, P., Björnberg, O., Nielsen, F. S., Jensen, K. F., Larsen, S. (1998) The crystal structure of *Lactococcus lactis* dihydroorotate dehydrogenase A complexed with the enzyme reaction product throws light on its enzymatic function, *Protein Sci. 7*, 1269−1279.
6. Rowland, P., Nørager, S., Jensen, K. F., and Larsen, S. (2000) Structure of dihydroorotate dehydrogenase B: electron transfer between two flavin groups bridged by an iron-sulphur cluster, *Structure 8*, 1227−1238.
7. Liu, S., Neidhardt, E. A., Grossman, T. H., Ocain, T., and Clardy, J. (2000) Structures of human dihydroorotate dehydrogenase in complex with antiproliferative agents, *Structure 8*, 25−33.
8. Nørager, S., Jensen, K. F., Björnberg, O., and Larsen, S. (2002) *E. coli* dihydroorotate dehydrogenase reveals structural and functional distinctions between different classes of dihydroorotate dehydrogenases, *Structure 10*, 1211−1223.
9. Hansen, M., Le Nours, J., Johansson, E., Antal, T., Ullrich, A., Löffler, M., and Larsen, S. (2004) Inhibitor binding in a class 2 dihydroorotate dehydrogenase causes variations in the membrane-associated N-terminal domain, *Protein Sci. 13*, 1031−1042.
10. Palfey, B. A., Björnberg, O., and Jensen, K. F. (2001) Insight into the chemistry of flavin reduction and oxidation in *Escherichia coli* dihydroorotate dehydrogenase obtained by rapid reaction studies, *Biochemistry 40*, 4381−4390.
11. Palfey, B. A., Björnberg, O., and Jensen, K. F. (2001) Specific inhibition of a family 1A dihydroorotate dehydrogenase by benzoate pyrimidine analogues, *J. Med. Chem. 44*, 2861−2864.
12. Nielsen, F. S., Rowland, P., Larsen, S., and Jensen, K. F. (1996) Purification and characterization of dihydroorotate dehydrogenase A from *Lactococcus lactis*, crystallization and preliminary X-ray diffraction studies of the enzyme, *Protein Sci. 5*, 852−856.
13. Otwinowski, Z., and Minor, W. (1997) Processing of X-ray diffraction data collected in oscillation mode, *Methods Enzymol. 276*, 307−326.
14. Nørager, S., Arent, S., Björnberg, O., Ottosen, Leggio, L. L., Jensen, K. J., and Larsen, S. (2003) *Lactococcus lactis* dihydroorotate dehydrogenase A mutants reveal important facets of the enzymatic function, *J. Biol. Chem. 278*, 28812−28822.

15. Murshudov, G. N, Vagin, A. A., and Dodson, E. J. (1997) Refinement of macromolecular structures by the maximum-likelihood method, *Acta Crystallogr., Sect. D 53*, 240−255.
16. Lamzin, V.S., Perrakis, A., and Wilson, K. S. (2001) in *International Tables for Crystallography: Crystallography of Biological Macromolecules* (Rossmann, M. G., and Arnold, E., Eds.) Vol. F, pp 720−722, Kluwer Academic Publishers, Dordrecht, The Netherlands.
17. Jones, S., and Thornton, J. M. (1996) Principles of protein-protein interactions, *Proc. Natl. Acad. Sci. U.S.A 93*, 13−20.
18. Dean, J. A., Ed. (1999) *Lange's Handbook of Chemistry*, 15th ed., McGraw-Hill, Inc., New York.
19. Baker, B. M., and Murphy, K. P. (1996) Evaluation of linked protonation effects in proteinbinding reactions using isothermal titration calorimetry, *Biophys. J. 71*, 2049−2055.
20. Christensen, J. J., Hansen, L. D., and Izatt, R. M. (1983) *Handbook of Proton Ionization Heats and Related Thermodynamic Quantities*, Wiley, New York.
21. Strickland, S., Palmer, G., and Massey, V. (1975) Determination of dissociation constants and specific rate constants of enzyme-substrate (or protein-ligand) interactions from rapid reaction kinetic data, *J. Biol. Chem. 250*, 4048−4052.
22. Gates, C. A., and Northrop, D. B. (1988) Determination of the rate-limiting segment of aminoglycoside nucleotidyltransferase 2″-I by pH- and viscosity-dependent kinetics, *Biochemistry 27*, 3834−3842.
23. Howell, E. E., Villafranca, J. E., Warren, M. S., Oatley, J. S., and Kraut, J. (1986) Functional role of aspartic acid-27 in dihydrofolate reductase revealed by mutagenesis, *Science 231*, 1123−1128.
24. Craik, C. S., Roczniak, S., Largman, C., and Rutter, W. J. (1987) The catalytic role of the active site aspartic acid in serine proteases, *Science 237*, 909−913.
25. Laskowski R. A., MacArthur M. W., Moss D. S., and Thornton J. M. (1993) PROCHECK: a program to check the stereochemical quality of protein structures, *J. Appl. Crystallogr. 26*, 283−291.
26. Morris A. L., MacArthur M. W., Hutchinson E. G., and Thornton J. M. (1992) Stereochemical quality of protein structure coordinates, *Proteins 12*, 345−364.
27. Vriend, G. (1990) WHAT IF: A molecular modeling and drug design program, *J. Mol. Graphics 8*, 52−56.
28. Rowland, P., Nielsen, F. S., Jensen, K. F., and Larsen, S. (1997) The crystal structure of the flavin containing enzyme dihydroorotate dehydrogenase A from *Lactococcus lactis*, *Structure 5*, 239−252.
29. Zheng, Y., Massey, V., Schaller, A., Palfey, B. A., and Carey, P. R. (2001) Comparison of resonance Raman spectra of flavin-3,4-dihydroxybenzoate charge-transfer complexes in three flavoenzymes, *J. Raman Spectrosc. 32*, 579−586.
30. Ottosen, M. B., Björnberg, O., Nørager, S., Larsen, S., Palfey, B. A., and Jensen, K. F. (2002) The dimeric dihydroorotate dehydrogenase A from *Lactococcus lactis* dissociates reversibly into inactive monomers, *Protein Sci. 11*, 2575−2583.
31. Marcinkeviciene, J., Jiang, W., Locke, G., Kophcho, L. M., Rogers, M. J., and Copeland, R. A. (2000) A second dihydroorotate dehydrogenase (type A) of the human pathogen *Enterococcus faecalis*: expression, purification, and steady-state kinetic mechanism, *Arch. Biochem. Biophys. 377*, 178−186.
32. Takashima, E., Inaoka, D. K., Osanai, A., Nara, T., Odaka, M., Aoki, T., Inaka, K., Harada, S., and Kita, K. (2002) Characterization of the dihydroorotate dehydrogenase as a soluble fumarate reductase in *Trypanosoma cruzi*, *Mol. Biochem. Parasitol. 122*, 189−200.
33. Zameitat, E., Knecht, W., Piskur, J., and Löffler, M. (2004) Two different dihydroorotate dehydrogenases from yeast *Saccharomyces kluyveri*, *FEBS Lett. 568*, 129−134.
34. Annoura, T., Nara, T., Makiuchi, T., Hashimoto, T., and Aoki, T. (2005) The origin of dihydroorotate dehydrogenase genes of kinetoplastids, with special reference to their biological significance and adaptation to anaerobic, parasitic conditions, *J. Mol. Evol. 60*, 113−127.
35. Inaoka, D. K., Takashima, E., Osanai, A., Shimizu, H., Nara, T., Aoki, T., Harada, S., and Kita, K. (2005) Expression, purification and crystallization of *Trypanosoma cruzi* dihydroorotate dehydrogenase complexed with orotate, *Acta Crystallogr., Sect. F 61*, 875−878.
36. Cordeiro, A. T., Feliciano, P. R., and Nonato, M. C. (2006) Crystallization and preliminary X-ray diffraction analysis of *Leishmania major* dihydroorotate dehydrogenase, *Acta Crystallogr., Sect. F 62*, 1049−1051.
37. Nara, T., Kamei, Y., Tsubouchi, A., Annoura, T., Hirota, K., Iizumi, K., Dohmoto, Y., Ono, T., and Aoki, T. (2005) Inhibitory action of marine algae extracts on the *Trypanosoma cruzi* dihydroorotate dehydrogenase activity and on the protozoan growth in mammalian cells, *Parasitol. Int. 54*, 59−64.
38. Sariego, I., Annoura, T., Nara, T., Hashimoto, M., Tsubouchi, A., Iizumi, K., Makiuchi, T., Murata, E., Kita, K., and Aoki, T. (2006) Genetic diversity and kinetic properties of *Trypanosoma cruzi* dihydroorotate dehydrogenase isoforms, *Parasitol. Int. 55*, 11−16.
39. Johnson, K. A. (1992) Transient-State Kinetic Analysis of Enzyme Reaction Pathways, in *The Enzymes* (Sigman, D. S., Ed.) 3rd ed., Vol. XX, pp. 1−61, Academic Press, New York.
40. Cha, S. (1968) A simple method for derivation of rate equations for enzyme-catalyzed reactions under the rapid equilibrium assumption or combined assumptions of equilibrium and steady state, *J. Biol. Chem. 243*, 820−825.
41. Fridovich, I. (1965) The competitive inhibition of uricase by oxonate and by related derivatives of *s*-triazines, *J. Biol. Chem. 240*, 2491−2494.

BI7001554